

Multiple scattering and attenuation corrections in Deep Inelastic Neutron Scattering experiments

J. Dawidowski, J.J. Blostein and J.R. Granada¹

¹*Consejo Nacional de Investigaciones Científicas y Técnicas,
Centro Atómico Bariloche and Instituto Balseiro,
Comisión Nacional de Energía Atómica,
Universidad Nacional de Cuyo,(8400) Bariloche, Argentina**

(Dated: October 11, 2018)

Abstract

Multiple scattering and attenuation corrections in Deep Inelastic Neutron Scattering experiments are analyzed. The theoretical basis is stated, and a Monte Carlo procedure to perform the calculation is presented. The results are compared with experimental data. The importance of the accuracy in the description of the experimental parameters is tested, and the implications of the present results on the data analysis procedures is examined.

I. INTRODUCTION

Since its creation in 1966 by Hohenberg and Platzmann¹, the Deep Inelastic Neutron Scattering (DINS) technique was considered the most direct probe of the momentum distribution of nuclei in condensed matter. The interest on this technique was further stimulated by subsequent developments, that showed that features attributed to the interference between the neutron and the proton could be observed in experiments made on hydrogen², thus determining the wave function of the protons directly from the experimental data. The availability of this technique as a customary research tool, opened in the last decade a new field for the investigation in condensed matter, and stirred up particular interest in the study of hydrogen dynamics, a topic for which this technique is particularly suitable. Despite the main activity in the field is held at Rutherford Appleton Laboratory (United Kingdom), contributions from different laboratories were also reported in the past^{3,4,5} and recently^{6,7,8,9}.

The technique basically consists in an energy analysis carried out through the use of neutron resonant filters in the range of a few electron-Volts, and it is based on pulsed neutron sources. The spectra are recorded in time channels, which for the purpose of the study of momentum distributions must be translated to a momentum variable, thus obtaining the so-called Neutron Compton Profile (NCP).

The theoretical basis of the technique was established by Sears¹⁰, who outlined the general procedure that must be employed to arrive to the NCP from the experimental data. Later, Mayers¹¹ established the conditions of validity of the usually employed approximations.

Recently, we re-examined the usual procedure to analyze the experimental data obtained from this technique^{12,13}, and suggested improvements in the analysis of experiments involving light nuclei¹⁴. In the cited reference, we showed that the method to obtain the momentum distributions is, in general, a non-trivial task that involves a thorough knowledge of the different components of the experimental setup. In particular, it is important to know the energy spectrum of the incident neutrons, the detector efficiency, as well as an accurate description of the filter total cross section. However, in the above mentioned work we did not examine the sample-dependent effects such as multiple scattering and attenuation, which must be previously accounted for, before any analysis is attempted. It is a very well-known fact that multiple scattering and attenuation effects can be important even if all the reasonable cautions are taken in the sample design, since some low-signal portion of the observed spectra could nevertheless be seriously affected¹⁵.

Multiple scattering corrections is a long-debated subject, and has been extensively treated in the literature. Following the pioneering works of Vineyard¹⁶, and Blech and Averbach¹⁷, Sears thoroughly established its theoretical basis¹⁸, stating the integrals that describe the contribution of the n-th scattering process to the observed spectrum. The complexity of its solution was successfully tackled by Copley¹⁹ who devised a Monte Carlo code, suited to a particular experimental situation. However, Copley's scheme could not be easily adapted to different kinds of experiments. On the other hand, the common knowledge in neutron scattering technique teaches that specific procedures must be devised for each particular experimental situation^{15,20}.

Therefore, there is a primary need of a customary correction tool for multiple scattering and attenuation effects in DINS experiments, that was only recently fulfilled. The authors have already presented numerical results from a new Monte Carlo code compared with experimental results in multiple scattering corrections in DINS experiments (see Refs.^{7,8,9}), and recently Mayers *et al.*²¹ introduced the details of a new Monte Carlo code, related with the experimental setup thoroughly described in Ref.²². The Monte Carlo procedure described in the mentioned work contains a series of assumptions that were carefully analyzed in several publications. In the first place it is considered that the neutron has a well-defined final energy corresponding to the maximum of the main absorption of the resonant filter. In a recent analysis²³ we showed that such distributions are far more complex than considering a single final energy, and depends on the time channel and the dynamics of the scattering species. The scattering angles in²¹ are generated considering a random isotropic distribution. The validity of such assumption was investigated in Ref.²⁴ showing that the results obtained from such approximation deviate significantly from the exact ones when considering incident neutrons in the epithermal range. Another approximation contained in the mentioned work the description of the total cross sections of the scattering system with a constant plus a '1/v' absorption scattering law, which can deviate significantly from the real behavior when considering molecular systems²⁵.

In this paper we present the fundamentals of our Monte Carlo procedure to account for multiple scattering and attenuation effects. Account is taken of the experimental details such as the energy spectrum of the incident neutrons, the resonant filter transmission and the efficiency of the detectors bank. Regarding the sample, inelastic scattering is taken into account employing suitable models for each analyzed case. The proposed model can be easily introduced as a double-differential cross section, either analytical or numerically, so a complete description of the energy-transfers and scattering angles are obtained. Experimental results of samples of different sizes are

shown, and the present code is benchmarked. The importance of an accurate model to describe the neutron-sample interaction is stressed, and finally implications of multiple scattering corrections on different situations are discussed.

II. BASIC FORMALISM

A basic description of the kind of experiments that we will analyze can be found in Ref.¹², so we will give only a brief account here. We will analyze the case a DINS experiment performed in a pulsed source with an inverse-geometry configuration, *i.e.* the resonant filter is placed in the path of the neutrons emerging from the sample. A typical experiment consists of alternative 'filter out' and 'filter in' measurements, whose difference gives the NCP in the time-of-flight scale.

We define E_0 as the incident neutron energy (characterized by a spectrum $\Phi(E_0)$), E its final energy, L_0 the source-sample distance, L_s the sample-detector distance and θ the scattering angle. The total time elapsed since the neutron is emitted from the source until it is detected, for a single-scattering event, is

$$t = \sqrt{\frac{m}{2}} \left(\frac{L_0}{\sqrt{E_0}} + \frac{L_s}{\sqrt{E}} \right), \quad (1)$$

where m is the neutron mass.

The resonant filter will be characterized by a total cross section $\sigma_F(E)$, a number density n and a thickness T , so the fraction of neutrons transmitted by it will be $\exp(-nT\sigma_F(E))$. If $\frac{d^2\sigma}{dEd\Omega}(E_0, E, \theta)$ is the sample double-differential cross section, then the difference count rate ('filter-out' minus 'filter-in') at time of flight t , will be^{12,26}

$$c(t) = \int_{\substack{E_{\text{inf}} \\ t=\text{const}}}^{\infty} dE_0 \Phi(E_0) \frac{d^2\sigma}{d\Omega dE}(E_0, E, \theta) \varepsilon(E) (1 - e^{-nT\sigma_F(E)}) \left| \frac{\partial E}{\partial t} \right| \Delta\Omega, \quad (2)$$

where $\varepsilon(E)$ is the detector efficiency, and $\Delta\Omega$ the solid angle subtended by the detector.

Integral (2) must be calculated at constant time, taking into account relationship (1) between E_0 and E , and the Jacobian $|\partial E/\partial t|$ must be evaluated at a fixed time²⁶. The lower limit of integration is determined by the condition that in the second flight path the neutron has infinite velocity, *i.e.* $E_{\text{inf}} = \frac{1}{2}mL_0^2/t^2$. It is worth remarking that Eq. (2) is a valid expression only if single scattering events would take place.

III. MULTIPLE SCATTERING

In this section we will give an outline of the basic equations which govern the multiple scattering processes of n-th order, that are employed in the Monte Carlo programs. For a more detailed treatment the reader is referred to¹⁵ and¹⁸.

We will suppose throughout this paper an isotropic sample. Let $S(Q, \omega)$ be the scattering law of the sample, E_0 and E the incident and final neutron energies (being \mathbf{k}_0 and \mathbf{k} their corresponding wave vectors), $d\Omega$ the element of solid angle in the direction of the scattered neutron, σ_b the bound-atom scattering cross section of the sample (considered monatomic), and N the number of scattering centers, then the double-differential cross section is

$$\frac{d^2\sigma}{d\Omega dE} = \frac{N\sigma_b}{4\pi} \frac{k}{k_0} S(Q, \omega), \quad (3)$$

defined as the average number of scattered neutrons with final energies between E and $E + dE$, and within a solid angle $d\Omega$, per unit incident flux. As usual we define $\mathbf{Q} = \mathbf{k}_0 - \mathbf{k}$ and $\hbar\omega = E_0 - E$. The integral of Eq. (3) over all angles and final energies gives the microscopic total cross section $\sigma(E_0)$.

The above definition corresponds to the ideal textbook case where there is not multiple scattering. Turning to the real case let us define the *macroscopic double-differential cross section* as the probability that an incident neutron with a wave-vector \mathbf{k}_0 will emerge from the sample with a wave-vector \mathbf{k} ¹⁸. In this definition we do not take into account neutrons non-interacting with the sample (i.e. transmitted). Its expression thus reads

$$\frac{d^2\Sigma}{d\Omega dE} = \frac{1}{4\pi A} \frac{k}{k_0} s(\mathbf{k}_0, \mathbf{k}), \quad (4)$$

where A is the cross-sectional area perpendicular to the incident beam. $s(\mathbf{k}_0, \mathbf{k})$ is an effective scattering function that admits a decomposition in a part due to singly-scattered neutrons in the sample $s_1(\mathbf{k}_0, \mathbf{k})$, another due to singly-scattered neutrons in the container $s_C(\mathbf{k}_0, \mathbf{k})$, and a third due to multiply scattered neutrons (with any combination of sample-container scattering events) $s_M(\mathbf{k}_0, \mathbf{k})$

$$s(\mathbf{k}_0, \mathbf{k}) = s_1(\mathbf{k}_0, \mathbf{k}) + s_M(\mathbf{k}_0, \mathbf{k}) + s_C(\mathbf{k}_0, \mathbf{k}). \quad (5)$$

The single scattering component s_1 is simply related with the scattering law through the relationship

$$s_1(\mathbf{k}_0, \mathbf{k}) = N\sigma_b S(Q, \varepsilon) H(\mathbf{k}_0, \mathbf{k}), \quad (6)$$

where $H(\mathbf{k}_0, \mathbf{k})$ is the first-order attenuation factor, defined as the fraction of single-scattered neutrons that fail to leave the sample due to multiple scattering and nuclear absorption¹⁸ or that are not detected due to the detector efficiency¹⁵. Expression (4) inserted into (2), gives the real NCP including multiple scattering components. Its calculation, will normally involve a numerical simulation based on the Monte Carlo method.

IV. MONTE CARLO CODE

In this section we will describe the numerical simulation devised for DINS experiments. Its fundamentals are based on Copley's method¹⁹, and they are extensively developed in²⁷ and²⁸.

A. Neutron Histories

Neutron histories are generated with an initial unity weight. The incident neutron energy is decided randomly using the experimental neutron spectrum as the probability distribution. The flight path x for a neutron with energy E is given by the probability

$$p(E, x) = \frac{\Sigma_t(E, x)\mathcal{T}(E, x)}{1 - \mathcal{T}(E, d)}, \quad (7)$$

where the probability has been biased so the neutron never gets out of the sample²⁷. In Eq. (7), $\Sigma_t(E, x)$ is the macroscopic total cross section of the sample-container set a distance x away from the neutron previous scattering position, taken in the current flight direction, $\mathcal{T}(E, x)$ is the fraction of noninteracting (transmitted) neutrons in that direction after traversing a distance x , and d is the distance to the sample surface in that direction. To compensate the bias in the probability, a weight is assigned to each neutron which decreases according to the transmitted fraction in the traversed path, being 1 the initial value. Given the weight at step $i - 1$ the weight at step i is calculated as²⁸

$$w_i = w_{i-1}(1 - \mathcal{T}(E, d)) \frac{\Sigma_s(E, 0)}{\Sigma_t(E, 0)}, \quad (8)$$

where $\Sigma_s(E, 0)$ and $\Sigma_t(E, 0)$ are the macroscopic scattering and total cross sections, respectively, at position $i - 1$ and its ratio indicates the probability that the neutron will not be absorbed in the considered path. A history is finished when the weight drops under a predetermined cut-off value, so the number of scattering events is not predetermined.

The assignment of new energies and flight directions is made via the use of model distributions for the double-differential cross sections of the sample and the container environments, normalized

with the total cross section at the current energy E_i ¹⁵

$$P(E_i, E, \theta) = \frac{N\sigma_b}{4\pi\sigma(E_i)} \frac{k}{k_i} S_{model}(Q, \omega). \quad (9)$$

B. Scoring

At each step, the contribution of the current history to the detectors is calculated for each time-of-flight channel t . The final energy E to be considered for this channel is obtained from¹⁵

$$t = \sqrt{\frac{m}{2}} \left(\frac{L_0}{\sqrt{E_0}} + \sum_{i=1}^N \frac{L_i}{\sqrt{E_i}} + \frac{L_s}{\sqrt{E}} \right) \quad (10)$$

where N is the number of scattering steps, and L_i is the flight path of step i , which was covered with an energy E_i .

The quantity to be scored is the current weight, times the transmission factor from the current position to the sample surface in the direction towards the detector position, times the filter absorption ratio, times the detector efficiency

$$z_i = w_i P(E_i, E, \theta) \mathcal{T}(E, d) (1 - e^{-nT\sigma_F(E)}) \epsilon(E). \quad (11)$$

It can be shown¹⁵ that the average of z_i after a large number of histories is the sought solution of Eq.(2) for the case of a macroscopic sample (Eq.(4)).

C. Summary of input data

The above described Monte Carlo procedure, requires a detailed description of the experimental setup and total cross sections of the involved materials. It also makes use of models for the scattering laws to describe the sample and container interaction with neutrons. Here we summarize the input data needed to perform it.

- Incident spectrum as a function of energy.
- Total cross section of the sample and the container materials as a function of the energy. These data must be tabulated in an energy range wide enough to cover not only the energies corresponding to the incident spectrum (epithermal energies), but also to consider the energy transfers after a number multiple scattering steps (typically thermal energies).

- Mean free path of the sample and the container as a function of energy.
- Detector bank efficiency as a function of energy.
- Input parameters for the chosen models to describe the scattering law of the sample and the container. Alternatively the models can be defined through a numerical input.
- Geometry parameters for the proposed experimental setup and sample environment.
- Total cross section of the resonant filter in an energy range comprising thermal neutrons (to give a good description of the '1/v' region ³⁶), to energies above the main resonance (to describe the lower time-of-flight channels).

V. EXPERIMENTAL SETUP

The experiments were performed at the Bariloche pulsed neutron source (Argentina). Neutrons, produced by the interaction of the electrons accelerated by the LINAC on a lead target, are moderated in a 4 cm thick polyethylene slab. A cadmium sheet is placed in the incident beam, to absorb thermal neutrons. The LINAC was operated at a 100 Hz rate. A collimated neutron beam 1 inch diameter was employed.

A schematic view of the of the DINS facility is shown in Fig. 1. A movable cylindrical indium filter 0.25 mm thick, is placed in the flight path of the scattered neutrons. The movement is controlled remotely to perform alternative 'filter-in' and 'filter-out' measurements every 10 minutes. The detector bank consists of six ³He proportional counters (10 atm filling pressure, 6 inch active length, 1 inch diameter) placed at a mean scattering angle of 56° . The detectors were covered with cadmium cylinders to minimize the background due to thermal neutrons. The flight-path lengths were 504 cm (source-sample distance), and 27.5 cm (sample-detector) respectively.

The incident spectrum, measured employing a ³He detector placed perpendicularly to the direct beam, is shown in Fig. 2 where the detector efficiency effect was accounted for. The detector bank efficiency was determined through the ratio of the spectrum of scattered neutrons on a lead sample

³⁶ Here we refer to the slow neutron regime, where the absorption cross section is inversely proportional to the neutron velocity. See Ref.²⁹.

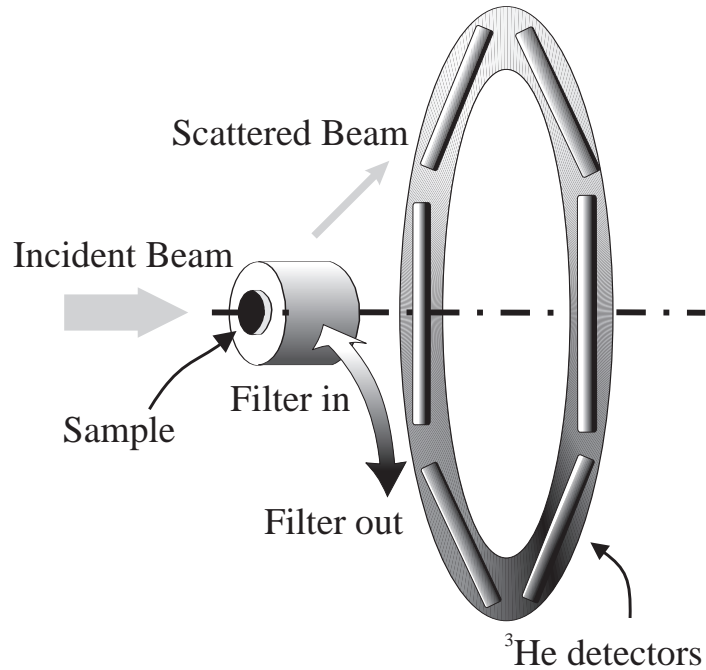


FIG. 1: Experimental setup employed for DINS experiments. The detectors are placed at a scattering angle of 56° .

(which is mostly an elastic scatterer), and the spectrum measured on the direct beam. The result is shown in Fig. 3 where the cutoff near 0.5 eV is due to the cadmium cylinders that cover the detectors.

VI. RESULTS AND DISCUSSION

In this section we will analyze our experimental and numerical results on the Compton profiles for coin-shaped graphite and polyethylene samples of different sizes at room temperature. In the further paragraphs we will show results on samples whose sizes were chosen to serve as a

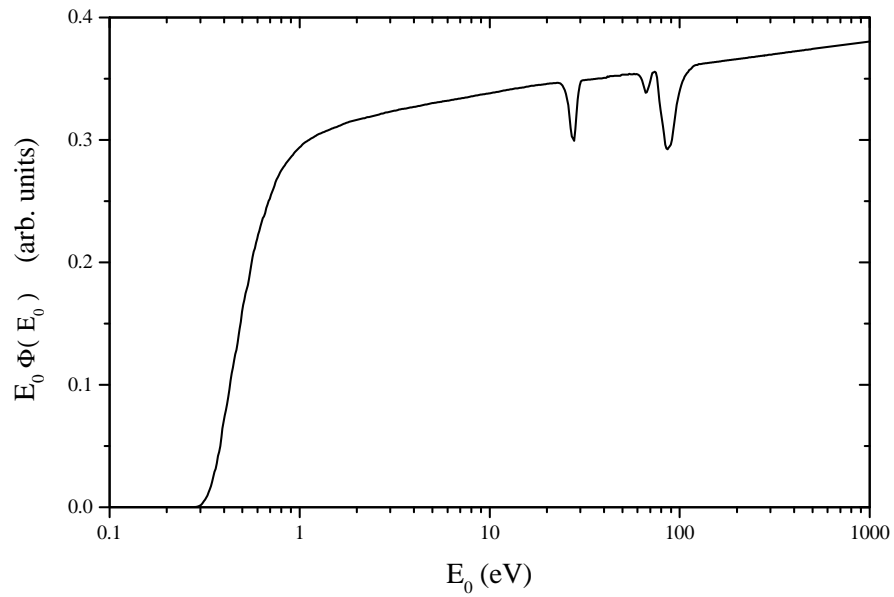


FIG. 2: Incident neutron spectrum multiplied by the energy in order to represent it in logarithmic E_0 scale. Dips due to resonances in the cadmium sheet are observed.

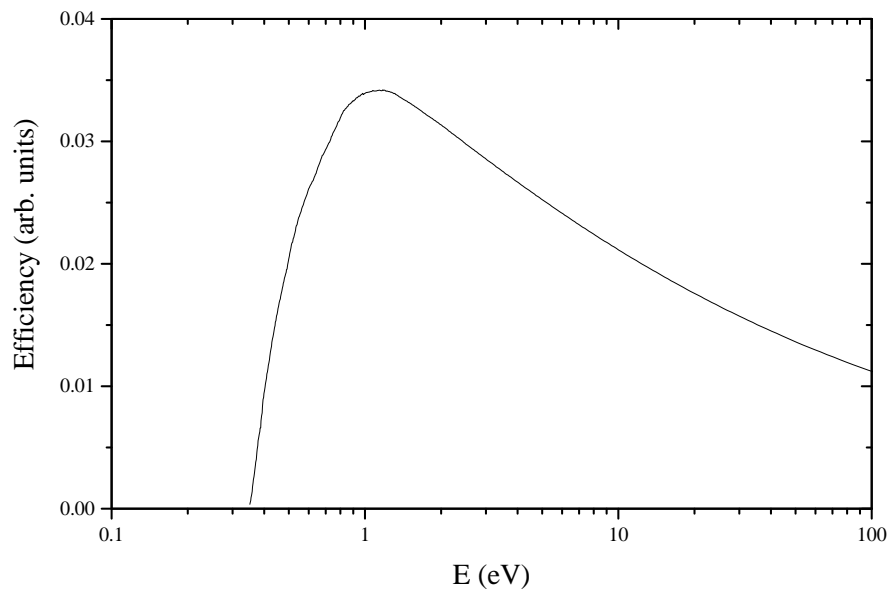


FIG. 3: Detector bank efficiency. The cutoff about 0.5 eV is due to the cadmium cylinders which cover the detectors.

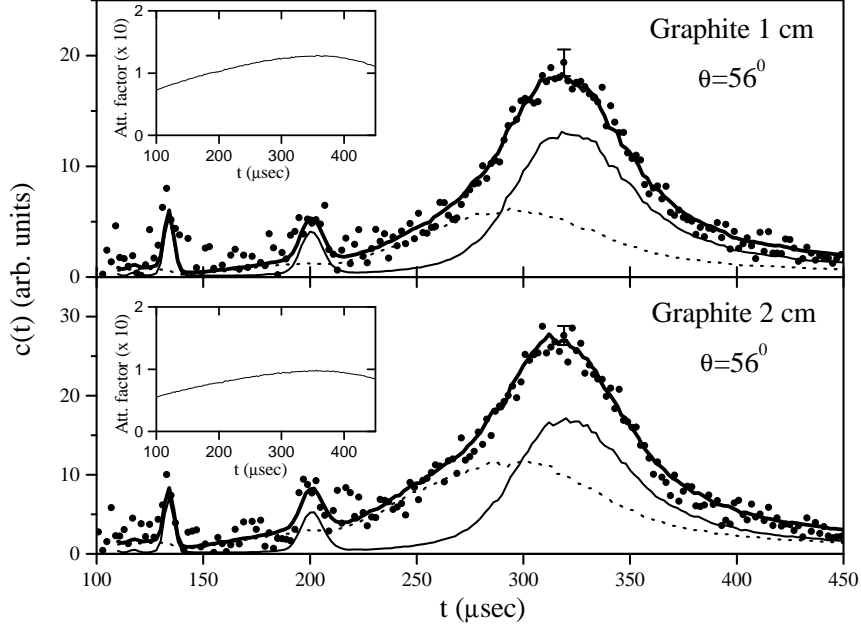


FIG. 4: NCP for the two measured graphite samples. Normal line: single scattering component; dotted line: multiple scattering; thick line: total scattering. Insets: attenuation factors

benchmark on the numerical simulations, and they are not intended to represent optimized choices in the experimental design. Finally we will show the importance of the present corrections in thin samples, suitable for the experimentalists' work. Numerical simulations were performed employing the above mentioned Monte Carlo code, making use of the experimental parameters mentioned in the previous section, and using total cross section data for the Indium filter from Ref.³⁰.

In Fig. 4 we show the results for the graphite samples, 3.54 cm diameter and 1 and 2 cm thickness respectively. A typical error bar is indicated for each experimental dataset. The approximate difference in count-rate ('filter out' minus 'filter in') at the peak maximum was 4 counts every 10000 LINAC pulses for the thin sample and 6 counts every 10000 LINAC pulses for the thick one. Measurements were carried out in 4 million LINAC pulses for the thin and 2 million LINAC pulses for the thick sample. Numerical simulations were carried out using a gas model for the graphite. This is a good approach at epithermal energies like in this case, with the condition that the temperature must be replaced by an effective temperature that takes into account the phonon dynamics³². The resulting effective temperature is 61.2 meV calculated on the basis of a Debye temperature of 1860 K³¹. In Fig. 4 we show the Monte Carlo results for the single and multiple

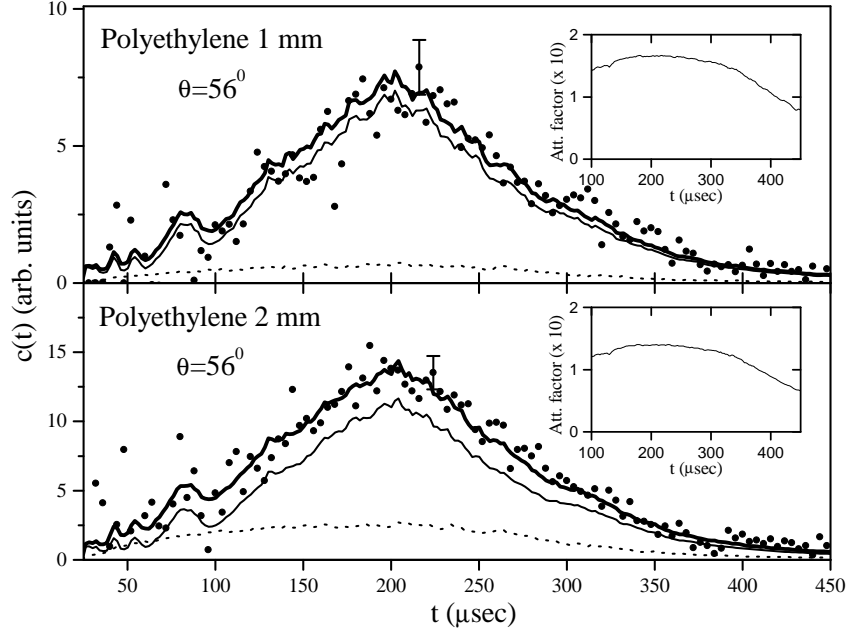


FIG. 5: NCP for the two measured polyethylene samples. The same notation as in Fig. 4 applies. Insets: attenuation factors

scattering components as well as the total one. Besides the main peak at about $315 \mu\text{sec}$ two extra peaks at 200 and $130 \mu\text{sec}$ are observed, due to the resonances of 3.85 and 9.07 eV of Indium, respectively. A good agreement is observed between the calculation and the experimental data, showing that the multiple scattering component has a peak shape that is broader than the main peak and is centered at lower times of flight, thus contributing to a significant distortion in the observed total scattering. In the insets of Fig. 4 we show the attenuation factors (Eq. (6)), that have to be applied to the observed profile, once multiple scattering is subtracted.

In Fig. 5 we show the same results for the two samples of polyethylene 3 cm diameter and 1 and 2 mm thickness respectively, where typical error bars are shown. The approximate count rate at the peak position was 5 counts every 10000 LINAC pulses for the thin sample and 7.5 counts every 10000 LINAC pulses for the thick one. Measurements were carried out in 5 million LINAC pulses for the thin and 4 million LINAC pulses for the thick sample. For the Monte Carlo simulations we employed the Synthetic Model²⁵ with the parameters from Ref.³³, which was successfully employed to describe different integral magnitudes of the double-differential cross section. The model adequately describes the interaction between the neutron and the sample in different energy regimes, tending naturally to the commonly employed impulse approximation in the epithermal

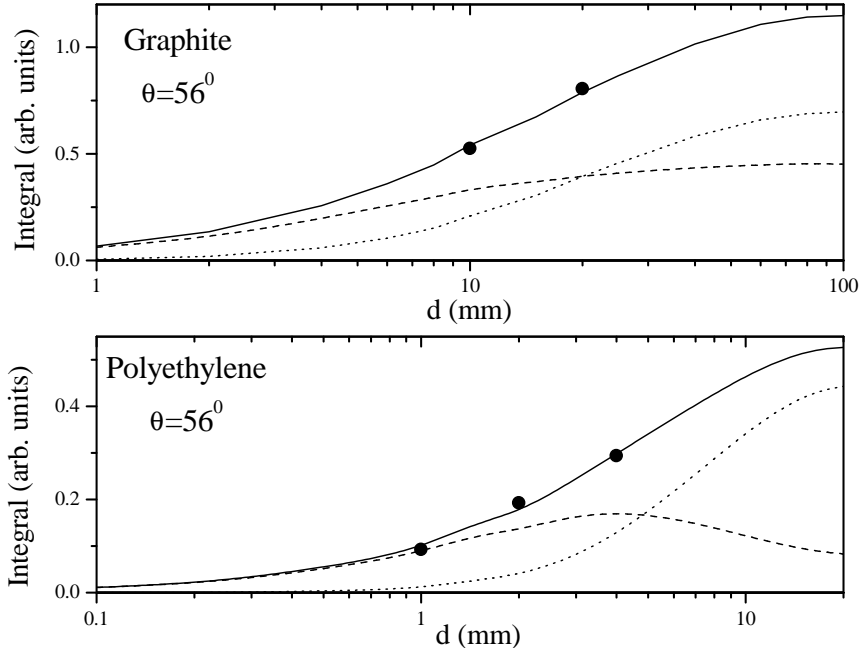


FIG. 6: Integrated intensity for single (dashed line), multiple (dotted line) and total scattering (full line) for different thicknesses of graphite and polyethylene samples, compared with the experimental data (black circles).

region. Although the shape of the observed main peak due to hydrogen is less affected by multiple scattering effects than in the case of graphite, it must be noted the distorting effect due to the attenuation factor that varies a 25 % from 200 to 350 μsec thus affecting significantly the long-times tail of the Compton profiles.

The general trend of the multiple scattering behavior can be analyzed by observing the total intensities observed in the main peak of the Compton profiles as a function of the sample thickness. In Fig. 6 we show the integral intensity of the main peak for single, multiple and total scattering obtained from Monte Carlo simulations at several sample thicknesses of graphite and polyethylene. In the same graph we show the results obtained from our experimental data. In the case of polyethylene, we measured a third sample 4 mm thick, that is not included in Fig. 5, but is shown in Fig. 6. It is worth to mention that the results from the simulations were multiplied by a constant (the same value in all the cases) in order to fit the experimental data. In both systems, we observe that the trend of the peak intensity as a function of the sample thickness can be correctly accounted for only if multiple scattering processes are considered.

It is worth to emphasize the importance of a good description of the filter total cross section and

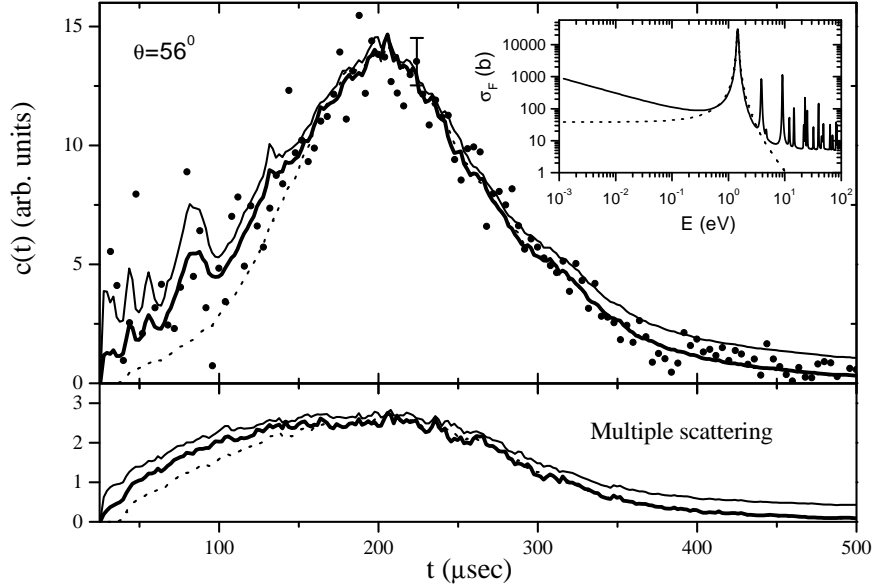


FIG. 7: Main frame: Comparison of the Monte Carlo run for a 2mm thick polyethylene sample (thick line) with a black detector model (thin line) and with a Lorentzian shape for the filter total cross section (dotted line) and the experimental data (dots). Lower frame: detail of the multiple scattering components. Inset: Lorentzian approach (dotted line) compared with the real total cross section for the indium filter (full line).

the detector efficiency. For that purpose we performed simulations assuming two different cases:

- (a) a black detector (*i.e.* a detector with unit efficiency) and the filter described by the complete absorption cross section;
- (b) a filter described with a Lorentzian shape³⁶, with the real detector efficiency.

In both cases commonly employed approaches are used. The results are shown in Fig . 7 and in the inset the Lorentzian used to represent the filter together with the exact cross section³⁰. We observe that both assumptions are inadequate and affect both the single and the multiple scattering components. In the case (a) the defect is manifested in an inaccurate description of the long-times tail. On the other hand, in (b) we observe an incorrect description in the short time region and the long-time tail, is mostly unaffected. It is worth to discuss the reason for both behaviors. The long-times region of the observed profile is mainly composed by emerging slow neutrons, which are absorbed by the filter according to the above referred '1/v' behavior. In the case of a black detector (a) our system is sensitive to those neutrons, while in (b) and our detectors are covered with

cadmium cylinders, whereby our detection system is insensitive to such neutrons. Both behaviors are observed in the calculated curves in Fig. 7, while experimental data only marginally illustrate the effect due to experimental errors.

Finally, it is worth to mention that in common practice, the experimentalist will choose an adequate sample size in order to minimize multiple scattering effects, while keeping an acceptable signal-to-noise ratio. To illustrate the multiple scattering and attenuation effects on samples suitable to the experimentalist, we present in Fig. 8 the results of our Monte Carlo program for thin sample thicknesses of graphite and polyethylene of the same diameters as presented in Figs. 4 and 5. In the upper frame we show our results for graphite (1 mm thick). We observe that although the multiple scattering contribution is small, it is non negligible, and it will have to be properly computed if accurate values of the peak-shape parameters are to be obtained from the experiment. Special attention must be paid to the attenuation factor, that still has an appreciable variation over the range of times of interest. The reason is that $H(\mathbf{k}_0, \mathbf{k})$ in Eq. (6) contains not only the attenuation in the sample (negligible for a thin sample) but also the fraction of detected neutrons (detector efficiency effects). In the case of polyethylene, we show the results of a 0.15 mm thick sample. The multiple scattering effect is barely visible, but the attenuation factor has also an appreciable variation over the range of interest, thus affecting the observed peak shape.

VII. DISCUSSION AND CONCLUSIONS

Throughout this paper we examined different aspects that affect multiple scattering and attenuation effects in DINS experiments. We presented a Monte Carlo procedure that adequately describes Multiple Scattering and attenuation processes in DINS experiments. To attain a good agreement between the numerical simulations and the experimental data, accurate descriptions of the incident neutron spectrum, the detector efficiency as a function of the energy and the filter total cross section were necessary. These considerations add up to those stated in Refs.^{12,13}, regarding the need of a good description of the experimental setup and the inadequacy of the convolution approximation in the description of the neutron Compton profiles. It must be remarked the importance of an accurate description of the efficiency of the detector system. As such, we understand the detecting setup that comprises the kind of detectors employed, the geometry and the materials involved. For instance, the detector system employed in this work is composed by ^3He tubes covered with cadmium, that result in the efficiency shown in Fig. 3. The importance of the knowl-

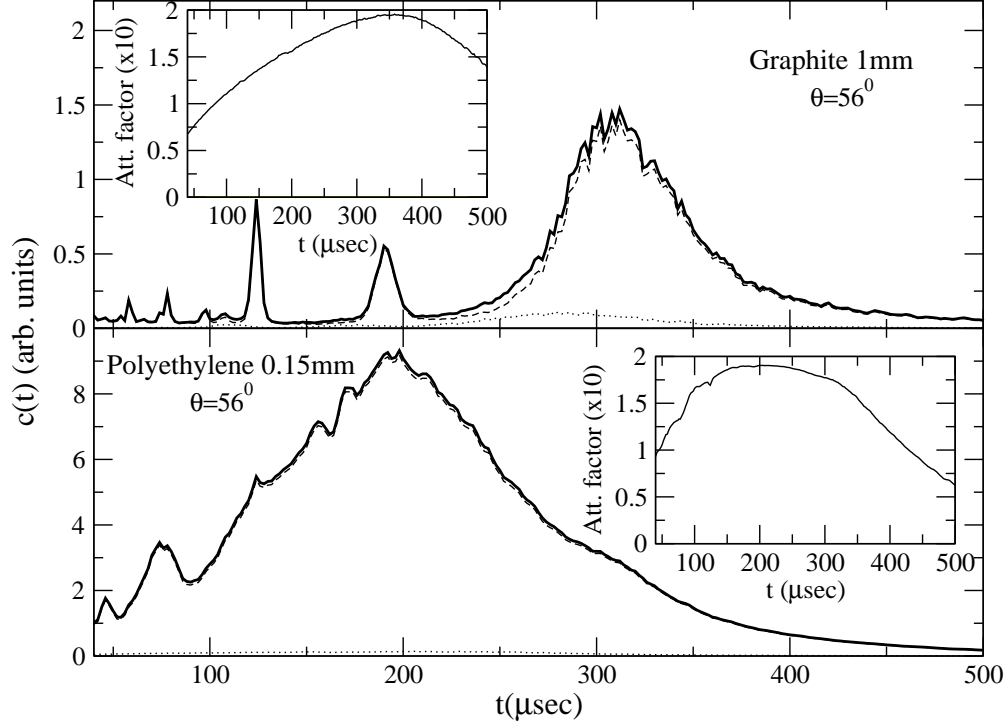


FIG. 8: NCP for thin graphite and polyethylene samples chosen to approach the experimentalists' needs. The same notation as in Fig. 4 applies. Insets: attenuation factors

edge of the detector efficiency as a function of the energy can be understood in the light of the recent work on the analysis of final energy distributions in DINS experiments²³. As a result of this analysis it was concluded that at every time of flight a distribution of final energies is operative in the neutron Compton profiles, instead of a single well-defined energy as is usually assumed in the customary data processing procedures²¹. As a consequence it is not sufficient to assume a detector operative at a single energy (in which case the knowledge of the efficiency function would be irrelevant), but the behavior of the efficiency function is essential, as confirmed by the results presented in Fig. 7.

The results presented on Multiple Scattering effects should be considered when designing a DINS experiment. In the analyzed graphite samples, the multiple scattering components have a significant structure that affect the shapes of the neutron Compton profiles. In the case of polyethylene, multiple scattering contributes with a flat background, but on the other hand the attenuation factor has a significant variation over the time range of interest. This is a consequence of the substantial variation of the efficiency function of our detection system in the range of energies shown in Fig. 3.

From the analyzed examples, we conclude that a wise choice of the sample thickness is still a valid rule, taking into account that a good contrast between ‘filter-out’ and ‘filter-in’ positions is required. Even if the sample sizes are adequately chosen, multiple scattering and/or attenuation corrections will necessarily have to be considered. The case of Fig. 8 is illustrative. Even if the multiple scattering contribution is small, the correction due to the attenuation factor can still be important (as shown in our case), given that it also includes the detectors’ efficiency correction¹⁵, which in our case has an appreciable variation with the energy. In general this result will depend on each particular detection system. All the considered cases show the need to perform accurate multiple scattering, attenuation and efficiency corrections. To this end numerical simulations are the most adequate procedure. In this paper we presented a suitable correction tool, for which an experimental benchmark with samples considerably affected by these corrections was satisfactorily performed.

These corrections will normally have to be taken into account before proceeding to the data analysis, *i.e.* obtaining the kinetic energy distributions of the atoms, peak areas, etc. Particular importance will have the corrections in the analysis of lighter nuclei. Monte Carlo simulations on heavier nuclei not shown in this paper²¹ reveal that the multiple scattering component tends to be located below the main peak and it is roughly proportional to it, thus having negligible distortion effects on its shape. This consideration must be brought together with those mentioned in Ref.¹² regarding the extreme care that must be exercised when analyzing light nuclei with the DINS technique.

VIII. ACKNOWLEDGEMENTS

We acknowledge Dr. R.E. Mayer for his collaboration during the experiments. We are especially grateful to L. Capararo, M. Schneebeli and P. D’Avanzo for the technical support. This work was supported by ANPCyT (Argentina) under Project PICT No. 03-4122, and CONICET (Project PEI 149/98).

* Electronic address: javier@cab.cnea.gov.ar

¹ P. C. Hohenberg and P.M. Platzmann, Phys. Rev. **152**, 198, (1966).

² J. Mayers, Phys. Rev. Lett. **71**, 1553, (1993).

- ³ R. M. Brugger, A. D. Taylor, C. E. Olsen, J. A. Goldstone and A. K. Soper, Nucl. Instr. and Meth. **221**, 393 (1984).
- ⁴ R. M. Brugger and P. A. Seeger, Nucl. Instr. and Meth. **A236**, 423 (1985).
- ⁵ H. Rauh and N. Watanabe, Nucl. Instr. and Meth. **222**, 507 (1984).
- ⁶ Y. Wang and P. E. Sokol, Phys. Rev. Lett. **72**, 1040, (1994).
- ⁷ J. Dawidowski, J. J. Blostein and J. R. Granada, in: M. R. Johnson, G. J. Kearley, H. G. Büttner (Eds.) Neutron and Numerical Methods, American Institute of Physics, New York, (1999), p. 37
- ⁸ J. J. Blostein, J. Dawidowski, J. R. Granada and R. E. Mayer, Appl. Phys. A **74** [Suppl.], S157 (2002).
- ⁹ J. J. Blostein, J. Dawidowski, and J. R. Granada, Proceedings of the 15th. International Collaboration on Advanced Neutron Sources, J. Suzuki and S. Itoh (Eds.), Tsukuba, Japan, (2000), p. 689.
- ¹⁰ V. F. Sears, Phys. Rev. B **30**, 44, (1984).
- ¹¹ J. Mayers, Phys. Rev. B **41**, 41, (1990).
- ¹² J. J. Blostein, J. Dawidowski and J. R. Granada, Physica B **304**, 357, (2001).
- ¹³ J. J. Blostein, J. Dawidowski and J. R. Granada, Physica B, **334**, 257 (2003).
- ¹⁴ J.J. Blostein, J. Dawidowski and J.R. Granada, Phys. Rev. B **71**, 054105 (2005).
- ¹⁵ J. Dawidowski, F. J. Bermejo and J. R. Granada, Phys. Rev. B **58**, 706, (1998).
- ¹⁶ G. M. Vineyard, Phys. Rev. **96**, 93, (1954).
- ¹⁷ I. A. Blech and R. L. Averbach, Phys. Rev. A **137**, 1113, (1965).
- ¹⁸ V. F. Sears, Adv. Phys. **24**, 1, (1975).
- ¹⁹ J. R. D. Copley, Comp. Phys. Comm. **7**, 289, (1974); J. R. D. Copley, P. Verkerk, A. A. Van Well and H. Fredrikze, Comp. Phys. Comm. **40**, 337, (1986).
- ²⁰ J. Dawidowski, J. R. Granada, R. E. Mayer, G. J. Cuello, V. H. Gillette and M.-C. Bellissent-Funel **203**, 116, (1994).
- ²¹ J. Mayers, A. L. Fielding and R. Senesi, Nucl. Instr. and Meth. A **481**, 454, (2002).
- ²² A. L. Fielding and J. Mayers, Nucl. Instr. and Meth. A **480**, 680, (2002).
- ²³ J. J. Blostein, J. Dawidowski and J. R. Granada, Nucl. Instr. and Meth. B (submitted, 2003).
- ²⁴ J. Dawidowski, G. J. Cuello and J. R. Granada, Nucl. Instr. and Meth B **82**, 459 (1993).
- ²⁵ J. R. Granada, Phys. Rev. B **31**, 4167, (1985).
- ²⁶ J. G. Powles, Mol. Phys. **26**, 1352, (1976).
- ²⁷ F. G. Bischoff, M. L. Yeater and W. E. Moore, Nucl. Sci. Eng. **48**, 266, (1972).
- ²⁸ J. Spanier and E. Gelbard, *Monte Carlo principles and neutron problems*, Addison Wesley, Reading,

(1969).

- ²⁹ J. M. Blatt and V. F. Weisskopf, *Theoretical Nuclear Physics*, Wiley, New York (1952), p. 470.
- ³⁰ V. McLane, C. L. Dunford and P. F. Rose, *Neutron Cross Sections*, Vol. 2, Academic Press, New York, 1988, p. 411.
- ³¹ N. W. Ashcroft and N. D. Mermin, *Solid State Physics*, Saunders College Publishing, 1976.
- ³² J. R. Granada, *Z. Naturforsch.* **39a**, 1160 , (1984).
- ³³ J. R. Granada, J. Dawidowski, R. E. Mayer and V. H. Gillette, *Nucl. Instr. Meth.* **A261**, 573, (1987).
- ³⁴ S. F. Mughabghab, M. Divadeenam and N. E. Holden, *Neutron Cross Sections*, Academic Press, Vol. 1, Part B, p. 79-1 (1981).
- ³⁵ K. H. Beckurts and K. Wirtz, *Neutron Physics*, Springer, Berlin, 1964, p. 134.
- ³⁶ A Lorentzian centered at 1.457 eV and full-width at half maximum of 0.2016 eV was employed. This value is greater than the one found in the literature³⁴ (0.075 eV at 0 K) due to the finite temperature of the filter. The peak shape at finite temperature is not a Lorentzian but a peak described with the Lamb equation³⁵ , that is broader due to the Doppler effect.